Thermal Stability of Shear-Induced Shish-Kebab Precursor Structure from High Molecular Weight Polyethylene Chains

Feng Zuo, Jong Kahk Keum, Ling Yang, Rajesh H. Somani, and Benjamin S. Hsiao*

Department of Chemistry, Stony Brook University, Stony Brook, New York 11794-3400

Received November 2, 2005; Revised Manuscript Received January 11, 2006

ABSTRACT: In-situ rheo-SAXS (small-angle X-ray scattering) and rheo-WAXD (wide-angle X-ray diffraction) techniques were used to investigate repeated melting and re-formation of the flow-induced shish-kebab precursor structure in a once-sheared polyethylene (PE) bimodal blend at the confined quiescent state. The blend consisted of a noncrystallizing low molecular weight PE matrix (LMWPE, $\bar{M}_w = 53\,000$ g/mol, polydispersity = 2.2) and a small amount (2 wt %) of crystallizing high molecular weight PE (HMWPE, $\bar{M}_w = 1\,500\,000$ g/mol, polydispersity = 1.1) under the chosen experimental temperature. After a step shear (shear rate = 125 s^{-1}, shear duration = 20 s, temperature = 126.5 °C), combined SAXS and WAXD results confirmed that the shish-kebab structure was developed mainly from HMWPE chains, following a diffusion-controlled-like process. Although shish formed first followed by microkebabs and then macrokebabs, shish and microkebabs were melted simultaneously as an integrated entity after the macrokebab melting. Upon cooling, the shish-kebab structure could re-form rather quickly from unrelaxed stretched chain segments, but the corresponding fraction decreased with the increase in temperature. Results indicated that the shish-kebab re-formation is directly related to the relaxation behavior of stretched chain segments confined in a topologically deformed entanglement network. Under the chosen experimental conditions, the deformed HMWPE entanglement network could withstand temperature until 154 °C for 3 min before totally relaxed into the isotropic state.

Introduction

The molecular mechanism, responsible for the formation of the initial crystallization precursor structure (i.e., shish-kebabs) induced by flow prior to the full scale crystallization process in entangled polymer melts, is an important subject, having many practical implications to polymer processing and property manipulation. It is thought that the topological arrangement of the shish-kebab precursors can directly influence the subsequent developments of crystallinity, crystallization rate, and morphology.[1−7] However, the subject is still not well understood. Recent studies from different laboratories all indicated that the high molecular weight species in the molecular weight distribution play an essential role of forming the precursor structure under flow in an entangled and supercooled melt.[8−14] In this study, our goals are thus twofold: (1) to demonstrate that, beyond any doubt, the shish-kebab structure is induced by the high molecular weight chains (even with a rather narrow polydispersity of 1.1) in a bimodal blend of low and high molecular weight polyethylene model samples under flow; (2) to explore the relationship between the thermal stability of the shear-induced shish-kebab structure and the relaxation behavior of deformed entangled high molecular weight chains at varying temperatures.

It is necessary to point out that the current state of theoretical development for the shish-kebab formation in entangled polymer melts under flow is primarily based on the concept of the stretch−coil transition for dilute polymer solutions proposed by de Gennes.[15] Keller adopted the stretch−coil transition concept for polymer melts and proposed the existence of a critical orientation molecular weight (M^*) under a particular flow field (e.g., extensional flow).[16,17] That is, the linear polymer chain having a molecular weight above the M^* value can remain in the stretched state after flow due to its long relaxation time, while shorter chains will relax back to the coiled state due to the corresponding short relaxation time. The critical molecular weight is related to the elongation rate as $\epsilon_c \propto (M^*)^{-\beta}$. On the basis of this argument, the high molecular weight species, which can remain in the stretched state upon deformation, are mainly responsible for the shish-kebab formation. However, Keller did not rationalize the obvious consequence of the high molecular weight chains; i.e., they possess a large number of chain entanglements. It is very unlikely that the stretch−coil transition can take place at the level of individual chain because multiple steps of chain disentanglement cannot occur under the typical flow conditions. Recently, the simulation work carried out by Muthukumar et al. showed that the shish-kebab structure can be formed by stretched and coiled chains, which coexist without stable intermediate conformations, in a monodispersed system under flow.[18] Of course, if one considers the scale of chain length for the high molecular weight species, the use of short monodispersed chains in simulation does not reflect the reality. However, if one considers the scenario of chain entanglement, the simulation with monodispersed chains would make perfect sense, as the average chain length between the entanglement points must be, statistically, about the same. Furthermore, if the entangled chains in a supercooled state can be considered as a network structure with slow dynamics, a uniaxial deformation field will induce orientation in the chain segments along the flow direction, resulting in the stretched chain segments between the entanglement points, but it will not affect the chain segments arranged perpendicularly to the flow.

In the literature, the melting behavior of the shish-kebab structure has been investigated quite extensively.[19−29] For example, Keller studied the changes of the shish-kebab structure in polyethylene using transmission electron microscopy (TEM) before, during, and after the melting process by rapid quenching or isothermal crystallization.[24−26] When the shish-kebab structure was heated to 130 °C, some kebabs started to melt and formed beads, while the shish fibril became smooth or blobby. Above 145 °C, kebabs totally disappeared, evidenced by the

* To whom correspondence should be addressed: e-mail bhsiao@notes.cc.sunysb.edu; Tel 631-632-7793; Fax 631-632-6518.

10.1021/ma052340g CCC: $33.50
Published on Web 02/23/2006

disappearance of the corresponding crystal reflections. If the molten sample was quenched, a smooth fiber could be obtained; but if the sample was slowly cooled and crystallized at a lower temperature, the molten beads could restore themselves into kebabs. It appeared that the chains within the melt−hairdressed-like fibrils could transform back to the initial shish-kebab structure, and the shish could retain the previous orientation. Petermann et al. also studied the partial melting of the shish-kebab structure of isotactic polystyrene with TEM.[27−29] Their results confirmed the existence of several components in the shish-kebab structure, including the central extended-chain microshish, the partially extended-chain macroshish, the microkebabs, and the overgrown macrokebabs. The macrokebabs that grew on the microkebabs templates were less thermally stable than microkebabs and, upon heating, became segmented and discontinuous, but the shish cores remained intact. It was thought that microkebabs originated from the firmly attached cilia to the shish backbone, having parts intrinsically implanted in the shish. These kebabs had a higher melting temperature, and at a high temperature, all kebabs completely melt, leaving behind only the more stable extended-chain shish. In fact, they observed that the shish could melt at a temperature beyond the equilibrium temperature of infinitely thick extended-chain crystals. Therefore, they argued that, since some kebabs have many tie chains that resemble micellar type of crystal structure, the hairdressing structure in Keller's model, which only accounts for the folded-chain kebab crystal growth, was incomplete. Upon cooling to lower temperatures, the partially melted kebabs reform again during isothermal crystallization. Although we do not disagree with the above viewpoints by Keller et al. and Peterman et al., in this study, we have attempted to further understand the molecular mechanism responsible for the thermal stability of the shish-kebab structure in an entangled melt, especially from the viewpoint of the relaxation of a deformed entangled polymer network.

To carry out this study properly, we have chosen a unique bimodal polyethylene blend, containing a very narrowly distributed high molecular weight component ($\bar{M}_w$ = 1 500 000 g/mol, polydispersity = 1.1), termed HMWPE, and a low molecular weight matrix ($\bar{M}_w$ = 53 000 g/mol, polydispersity = 2.2), termed LMWPE. The molecular weight of HMWPE is above the critical orientation molecular weight according to our group's previous work,[30,31] while the molecular weight of the LMWPE matrix is definitely below it. In addition, the chosen experimental temperature was such that LMWPE did not crystallize; only HMWPE crystallized. Thus, the bimodal blend was analogous to a dilute polymer solution having a high molecular weight crystallizing component with very slow chain dynamics (or long relaxation times) in a low molecular weight amorphous polymer matrix under the experimental conditions. The formation of the shish-kebab structure in the HMWPE component under shear and the corresponding shish-kebab structure thermal stability, by a thermal cycling method under planar constraints,[32] were investigated by in-situ rheo-SAXS (small-angle X-ray scattering) and rheo-WAXD (wide-angle X-ray diffraction) techniques with synchrotron radiation. As this study allowed us to follow only the crystallization, melting, and relaxation of HMWPE chains, some new insights into the shish-kebab formation under flow and its relationship with the dynamics of entangled melt of high molecular weight chains were obtained.

Experimental Section

Materials and Sample Preparation. Two polyethylene samples (LMWPE and HMWPE) were chosen for this study. LMWPE was an experimental polyethylene copolymer ($\bar{M}_w$ = 53 000 g/mol, polydispersity = 2.2), containing 2 mol % of hexane unit, and was provided by the ExxonMobil Research and Engineering Co., Annandale, NJ. The HMWPE sample ($\bar{M}_w$ = 1 500 000 g/mol, polydispersity = 1.1) was purchased from the Chevron Phillips Chemical Co. LP, Woodlands, TX. This sample was produced by a fractionation method. The sample information such as molecular weight, molecular weight distribution ($\bar{M}_w/\bar{M}_n$), nominal melting temperature, and end melting temperature ($T_{m,end}$ from DSC) are shown in Table 1, and their GPC profiles are shown in Figure 1. These model samples, all prepared by a metallocene catalyst, were used to prepare the bimodal polyethylene blend. The blend sample had a 2 wt % concentration of the HMWPE, which was higher than the overlap concentration (c^*) of HMWPE (c^* = 0.35 wt % according to the equation $c^* = 3\bar{M}_w/(4\pi[\langle R_g^2\rangle^{1/2}]^3 N_a)$, where $\langle R_g^2\rangle^{1/2}/\bar{M}_w^{1/2}$ was about 0.46, estimated form the SANS measurement).[33,34]

Table 1. Information about the Molecular Weight and the Melting Temperature of LMWPE and HMWPE

samples	$\bar{M}_w$ (g/mol)	MWD ($\bar{M}_w/\bar{M}_n$)	T_m (°C)[b]	$T_{m,end}$ (°C)[b]
LMWPE[a]	53 000	2.2	116	124
HMWPE	1 500 000	1.1	132	145

[a] Polymerized with 2 mol % of hexene comonomer using a metallocene catalyst. [b] The melting peak and end-of-melting temperature were obtained from DSC at a heating rate of 30 °C/min.

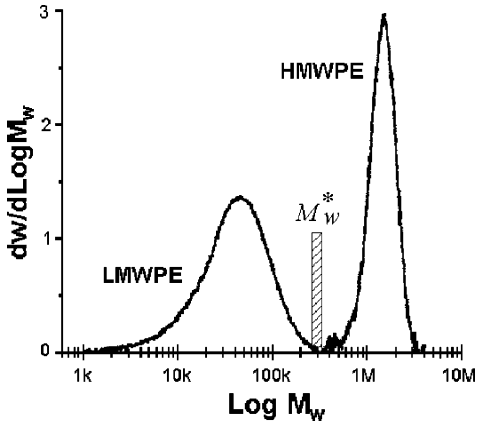

Figure 1. GPC profiles of LMWPE and HMWPE before blending. The range of M_w* represents the rough molecular weight values, which are near the critical orientation molecular weight according to our previous studies.[30,31]

The polymer blend was prepared by a solution mixing procedure to ensure the intimate blending of different species at the molecular level. The detailed mixing procedures can be found in our previous publication.[35] A control sample of pure LMWPE without the addition of HMWPE was also prepared using the same procedure. Polymer films of about 0.5 mm thickness were prepared by compression-molding at 150 °C. Samples in the form of a ring (inner diameter = 10 mm, outer diameter = 20 mm) were cut from the melt-pressed films for rheo-X-ray measurements.

Instrumentation. A Linkam CSS-450 optical shear stage, modified for in-situ rheo-X-ray studies, was used to apply controlled shear conditions to the polymer melt. The details of this modified shear apparatus have been described elsewhere.[36] Briefly, the sample was placed in the gap between two X-ray windows (i.e., a diamond window and a Kapton window) and completely enclosed in cavity of the measuring cell. WAXD and SAXS measurements were carried out at the X27C beamline in the National Synchrotron Light Source (NSLS), Brookhaven National Laboratory (BNL). The wavelength of the synchrotron radiation was 1.371 Å. 2D SAXS/WAXD patterns were collected by MAR CCD X-ray detector (MAR-USA), which had a resolution of 1024 × 1024 pixels (pixel size = 158.44 μm). For SAXS measurements, the sample-to-detector distance was 2014 mm, and the scattering angle was calibrated by silver behenate (AgBe); for WAXD measurements, the sample-to-detector distance was 109 mm, and the diffraction

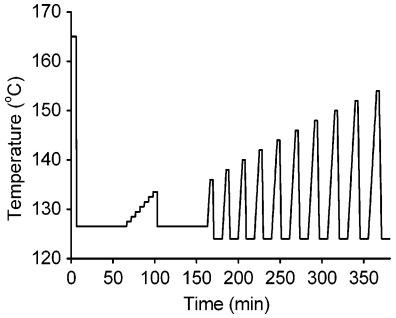

Figure 2. Thermal cycling protocol of this study. A step shear pulse was applied for 20 s (shear rate = 125 s^{-1}), after the collection of first SAXS or WAXD image upon the melt being cooled from 165 to 126.5 °C.

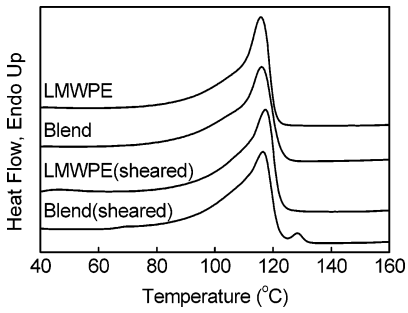

Figure 3. DSC melting thermograms of quiescently crystallized and shear-induced crystallized LMWPE and LMWPE/HMWPE blend samples (heating rate = 30 °C/min).

angle was calibrated by aluminum oxide (Al_2O_3). All X-ray images (SAXS and WAXD) were corrected for background scattering, air scattering, and beam fluctuations.

Differential scanning calorimetry (DSC) measurements were carried out using a Perkin-Elmer DSC 7 instrument. The chosen heating and cooling rates were the same, i.e., 30 °C/min. All DSC runs were carried out under a nitrogen gas flow to minimize sample oxidation. An indium standard was used to calibrate the temperature.

Experimental Procedure. To ensure that the polymer melt was free of any memory effects associated with the prior thermal and mechanical history, all polymer samples were subjected to the temperature protocol shown in Figure 2. The sample was first heated to 165 °C (substantially above the equilibrium melting temperature of polyethylene, $T_m° \approx 145$ °C, as well as the relaxation temperature of the entanglement network for HMWPE chains at 154 °C, which will be discussed later) and held for 5 min. The melt was then cooled to the chosen crystallization temperature of 126.5 °C at a 30 °C/min rate. Upon reaching the crystallization temperature, a SAXS or WAXD pattern was collected before the application of shear. Time-resolved X-ray images were subsequently taken upon the cessation of the applied shear (shear rate = 125 s^{-1}, shear duration = 20 s; shear duration was long enough to be in the zone of the steady-state behavior). The data acquisition time was 15 s, and the data storage time was 5 s for each scattering pattern for SAXS measurements; the data acquisition time was 22.5 s, and the data storage time was 7.5 s for WAXD measurements. After 1 h at the isothermal condition, thermal cycles were applied on the once-sheared melt under planar constraints in the Linkam stage to examine the thermal stability of shish-kebabs and its relationship with the relaxation of the deformed entanglement network of HMWPE chains. In the first thermal cycle, the shear melt was heated at a heating rate of 1 °C/min, but discontinuously or in several steps, to a temperature of 133.5 °C. At each intermediate step or temperature, the sample was held for 5 min for completion of the melting process. After the final step of melting at 133.5 °C, the sample was cooled to 126.5 °C at 30 °C/min and held there for 60 min. A sequential cycling thermal treatment for the study of the thermal stability of the shish-kebab structure was introduced as follows. In the next or second thermal cycle, the temperature was elevated at a 3 °C/min heating rate to a temperature that was about 2−2.5 °C higher than the highest temperature of the previous cycle (i.e., the cycle number and the corresponding highest temperature were as follows: for first cycle, 133.5 °C; second cycle, 136 °C; third cycle, 138 °C; and so on). At the final temperature of each cycle (second and higher), the melt was always equilibrated for 3 min and then subsequently cooled at a 10 °C/min rate to 124 °C, under which the melt was allowed to crystallize for 10 min. The sample was subjected to sequential thermal cycles until the final temperature of 154 °C, as shown in Figure 2. SAXS images were continuously collected during each cycle. The usefulness of the adopted, rather complex, thermal protocol was that it allowed us to precisely track melting and recrystallization (which can be related to the relaxation and memory of the constituent chain sections) of each component of the shish-kebab structure; namely, shish, microkebabs, and macrokebabs.

Results

DSC Evaluation of the Referenced Thermal Behavior in Sheared Samples. DSC melting thermograms for quiescently crystallized samples of pure LMWPE and the LMWPE/HMWPE blend (98:2) are shown in Figure 3. The samples were first heated to 165 °C for 5 min to erase thermal history and then cooled at 30 °C/min to room temperature. Both samples exhibited the same melting behavior, i.e., having a melting point around 115.8 °C; neither the second endotherm peak nor the broadening of the first endotherm peak was observed. This indicates that LMWPE and HMWPE were completely mixed at the molecular level and might have cocrystallized upon cooling (we note that the pure HMWPE sample exhibited a much higher melting point at 132.0 °C in DSC; data are not shown here). DSC melting thermograms for the once-sheared pure LMWPE and LMWPE/HMWPE blend samples are also shown in Figure 3. The initial samples were also heated to 165 °C for 5 min to erase thermal history, but after being cooled at 30 °C/min to 126.5 °C, they were subjected to a step shear (shear rate = 125 s^{-1}, shear duration = 20 s), held there 60 min for crystallization, and then cooled again at 30 °C/min to room temperature. The endotherm of the sheared LMWPE sample was almost the same as those of LMWPE and LMWPE/HMWPE blend crystallized under the quiescent state. However, the thermal behavior of the sheared LMWPE/HMWPE blend was very different, where two discrete peaks were seen during heating. The peak at lower temperature (115.8 °C) was due to the melting LMWPE, whereas the peak at higher temperature (128.4 °C) could be attributed to the shear-induced shish-kebab structure of HMWPE.

Rheo-WAXD Examination of Shear-Induced Crystallization by HMWPE Chains. Time-resolved WAXD patterns were collected for both LMWPE and LMWPE/HMWPE blend samples, which were crystallized at 126.5 °C for 60 min under both conditions with and without the application of shear at the beginning of crystallization. All WAXD patterns for LMWPE exhibited a diffuse scattering halo with no sign of crystal diffraction, confirming that the LMWPE chains remained in the molten amorphous state at 126.5 °C under and after shear. WAXD patterns for the LMWPE/HMWPE blend without shear exhibited a single isotropic crystal diffraction ring, which could be indexed as the (110) reflection at $2\theta = 25.54°$ (the wavelength was converted to 1.54 Å) from HMWPE crystals without preferred orientation.

Figure 4 shows selective 2D WAXD patterns of LMWPE/HMWPE blend before and during shear-induced crystallization at different times after the cessation of shear (shear rate = 125

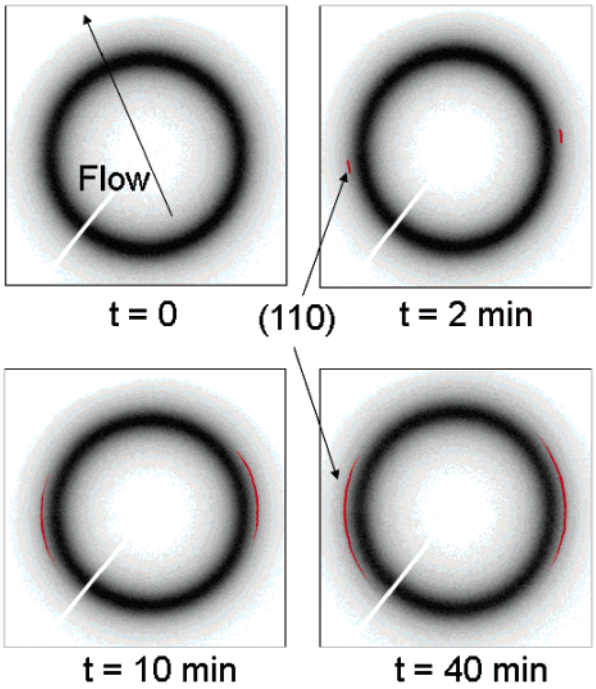

Figure 4. Selected 2D WAXD patterns (the (110) reflection peaks are filled in red to give a better contrast) of the LMWPE/HMWPE blend before the application of shear and during isothermal crystallization at 126.5 °C after cessation of shear (shear rate = 125 s^{-1}, shear duration = 20 s).

s^{-1}, shear duration = 20 s, temperature = 126.5 °C). The first pattern collected before the application of shear exhibited a diffuse scattering halo, similar to that of the molten LMWPE matrix. This observation indicated the presence of a completely amorphous melt, confirming the thermal clearing of all residual crystalline structures. The first appearance of the crystal diffraction (i.e., the equatorial (110) reflection) in WAXD from an orientated structure was seen at 2 min after the cessation of shear. This pattern exhibited a pair of sharp equatorial (110) reflections, which could be attributed to the shish formation with extended-chain crystals. A pair of weak (200) reflections was also detected, but its intensity was too low to be analyzed even after crystallization for 60 min. At longer times (e.g., t = 10 min), the azimuthal breadth of the (110) reflection was found to broaden significantly; a closer inspection revealed that it consisted of two discrete peaks with the corresponding azimuthal distribution: (1) the initially formed peak with a narrow azimuthal distribution (point-like) and (2) the subsequently developed peak with a broad azimuthal distribution (arc-like). The evolution of the diffraction pattern suggested the sequential formation of the shish-kebab structure; i.e., shish formed first followed by the growth of kebabs. This behavior is consistent with our previous observations of another similar blend that consisted of noncrystallizing LMWPE (termed MB-50K in the previous study) and crystallizing ultrahigh molecular weight polyethylene chains.[41] As no off-axis (110) reflection was observed, we concluded that the subsequently formed kebabs were not twisted because the twisted lamellae (kebabs) should produce four-arc off-axis (110) reflections. As expected, the total intensity of the reflections became stronger with time. At the end of the crystallization (time = 60 min), the total crystallinity estimated from the diffraction profile reached about 1%. This supports our hypothesis that LMWPE remains as an amorphous melt under the experimental conditions, and the observed crystallinity mainly results from HMWPE. It is reasonable to extrapolate the situation at longer crystallization times, where the crystallinity would be higher but less than 2%, which is the composition limit of the blend.

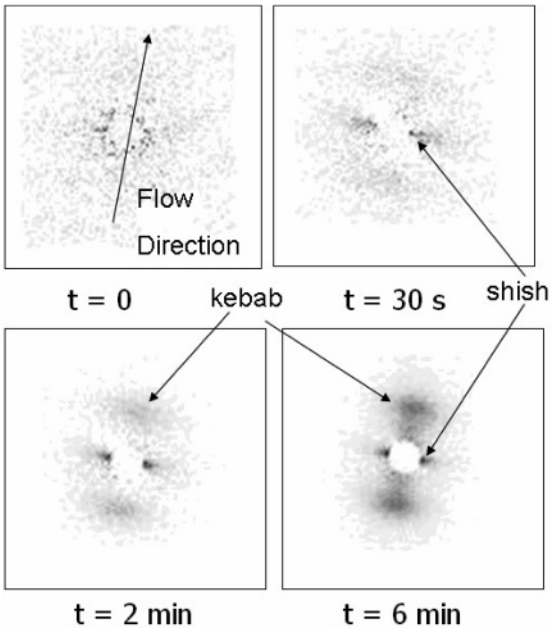

Figure 5. Selected 2D SAXS patterns of the LMWPE/HMWPE blend before the application of shear and during isothermal crystallization at 126.5 °C after the cessation of shear (shear rate = 125 s^{-1}, shear duration = 20 s).

Rheo-SAXS Study of Shear-Induced HMWPE Precursor Structural Development. Confirmation of the shish-kebab structure by SAXS. SAXS patterns of pure LMWPE with and without shear and those of the LMWPE/HMWPE blend without shear were first collected as reference experiments. These SAXS results were consistent with WAXD results, whereby all collected SAXS patterns did not exhibit any scattering features, indicating the absence of any ordered structures in the LMWPE melt with or without shear and in the LMWPE/HMWPE melt without shear at 126.5 °C.

Selective 2D SAXS patterns of the LMWPE/HMWPE blend before and after shear (shear rate = 125 s^{-1}, shear duration = 20 s, temperature = 126.5 °C) are shown in Figure 5. The SAXS pattern of the sheared LMWPE/HMWPE blend exhibited a clear equatorial streak arising immediately after the cessation of shear (at t = 30 s). The appearance of the equatorial streak indicated the formation of shish, containing extended crystals formed from the bundles of stretched chain segments parallel to the flow direction. The SAXS results were consistent with the WAXD results. Soon after the shish formation, strong scattering maxima appeared on the meridian. The meridional maximum could be attributed to the kebab growth, resulting from folded-chain crystallization. The oriented scattering features from the shish-kebab structure became stronger with the increase in time. Time evolution of the integrated scattered intensities from the shish and kebab fractions (I_{shish} and I_{kebab}) is illustrated in Figure 6. Both scattered intensities increased with the growth of shish-kebab structure. The higher I_{shish} value at the very beginning of the shear-induced crystallization than the corresponding I_{kebab} value (see Figure 6 inset) was because the shish was formed first and then the kebabs. The ratio of I_{kebab} to I_{shish} became about 3 at the end of crystallization.

Time evolution values of the average diameter of kebab is shown in Figure 7. These were estimated from a shish-kebab model analysis of the meridional intensity profile. The details of the analytical schemes were given elsewhere and would not

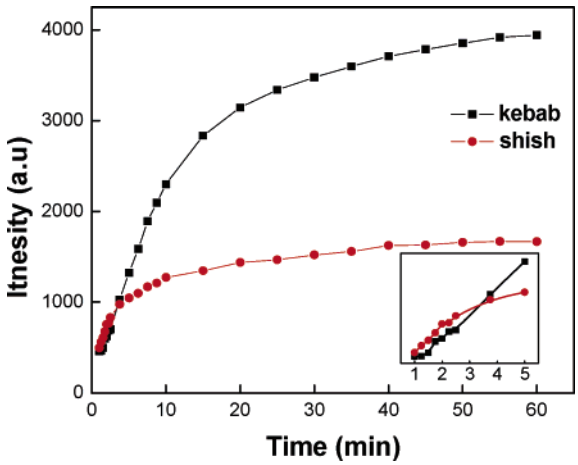

Figure 6. Time evolution of the integrated SAXS intensities from shish and kebabs in the LMWPE/HMWPE blend after shear. The inset shows the initial stage (shear rate = 125 s^{-1}, shear duration = 20 s).

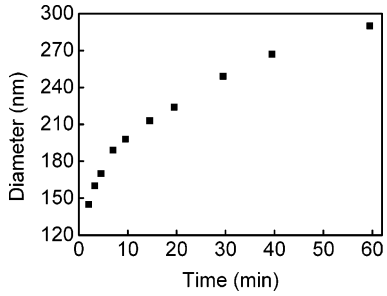

Figure 7. Time evolution of the average kebab diameter in the LMWPE/HMWPE blend after shear (shear rate = 125 s^{-1}, shear duration = 20 s).

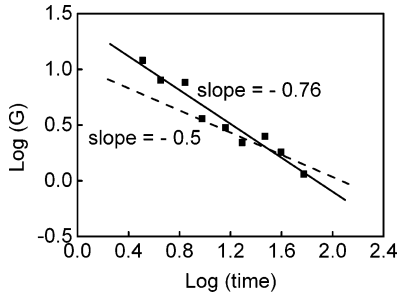

Figure 8. Average growth rate G of the kebab diameter in the LMWPE/HMWPE blend after shear. Results indicate the kebab growth follows diffusion-controlled-like process.

be repeated here.[37] It was found that the average diameter of the kebab increased with time, but not in a linear fashion (i.e., the kebab growth rate was not constant). The profile of the kebab growth rate ($G = dD/dt$, where D represents the kebab diameter and t is time) versus time on a logarithmic scale is plotted in Figure 8. The line in Figure 8 has a slope of −0.76; it roughly follows the relationship of $\log G \propto (-0.5)\log t$ for a diffusion-controlled growth process, predicted by Muthukumar et al.[18]

Melting and re-formation of the shish-kebab structure. After crystallization for 60 min at 126.5 °C, the once-sheared LMWPE/HMWPE sample was subjected to the first thermal cycle. Selected 2D SAXS patterns during this cycle are shown in Figure 9. It was found that with the increase of temperature the scattered intensity from the shish-kebab structure decreased accordingly, due to melting. The integrated scattered intensities (I_{shish} and I_{kebab}) at the end of each holding temperature are plotted in Figure 10a, showing that both values of I_{shish} and I_{kebab} decreased with the increasing temperature. When the temperature was elevated to 133.5 °C, both I_{shish} and I_{kebab} became zero. Although this appears to indicate the complete melting of the shish-kebab structure, it is not a conclusive evidence of whether the constituent chains have completely relaxed, as discussed below.

Figure 10b illustrates the time evolution of I_{shish} and I_{kebab} during heating and holding at the late stage of the first thermal cycle. It was interesting to see that during the heating process in this cycle, even with the increase of 1 °C, corresponding scattered intensities from shish and kebabs decreased rapidly. However, as soon as the sample was equilibrated at a constant temperature for a period of 5 min, both scattered intensities (I_{shish} and I_{kebab}) increased slightly, indicating the re-formation of some melted crystals. Overall, the changes of integrated scattered intensities for I_{shish} and I_{kebab} exhibited a steplike behavior, consistent with the steps in the thermal cycles. Figure 10c illustrates the ratio of I_{kebab} and I_{shish} at the end of each holding temperature, in which the ratio decreased slowly at lower temperatures and more rapidly (from 3 to 2) when the temperature approached 133.5 °C. It was interesting to note that the corresponding long period remained about constant at 40 nm during the heating and holding steps in the first thermal cycle (Figure 11). The above observations suggest the following sequence of events during melting of the shish-kebab structures: the less thermally stable macrokebabs melt first, followed by the simultaneous melting of shish and more thermally stable microkebabs. The detailed explanations for the above results are given in the Discussion section.

At the end of the first thermal cycle, the once-sheared sheared LMWPE/HMWPE blend was cooled continuously from 133.5 to 126.5 °C at 30 °C/min. This step revealed a very interesting behavior of the previously melted shish-kebabs. It was found that the shish-kebab structure re-formed. The SAXS patterns in Figure 9 (bottom) clearly evidenced a substantial re-formation of the prior structure. The overall scattering feature of the re-formed SAXS pattern at 126.5 °C was similar to that of the initial SAXS pattern. On the other hand, there were some subtle but notable differences between the two. Comparison of the SAXS patterns collected at 30 s and 126.5 °C, one after shear (Figure 5) and one during recrystallization (Figure 9), showed that the crystallization rate in the early stage of the recrystallization was much faster than that after shear. In fact, the scattered intensity of the SAXS pattern at 30 s during the recrystallization period was very close to that obtained about 4 min after shear. This could be explained by the difference in the state of orientation in the stretched chain segments, immediately after shear and after the melting of shish crystals. Let us first consider the process of melting. We argue that it follows a more or less reversible path; i.e., the structures that grow late melt first. Also, even after melting of the crystalline structures, the relaxation dynamics of the constituent chains of the underlying network/scaffold is very slow at the experimental conditions of temperature compared with the holding time. Chronologically, the chains in the initially formed structures, especially the primary nuclei (shish), will be the last to lose their state of orientation or conformation. Thus, a high fraction of the primary nuclei survive in the supercooled melt. In contrast, immediately after shear, it takes a certain time for the oriented chain segments to organize and form primary nuclei. As a result, crystallization kinetics in the recrystallization process was faster than that after shear. Also, it was found that the long period decreased slightly at the initial stage of recrystallization, and it reached a constant value at about 46 nm which was larger than the long period before the first thermal cycle (~40 nm).

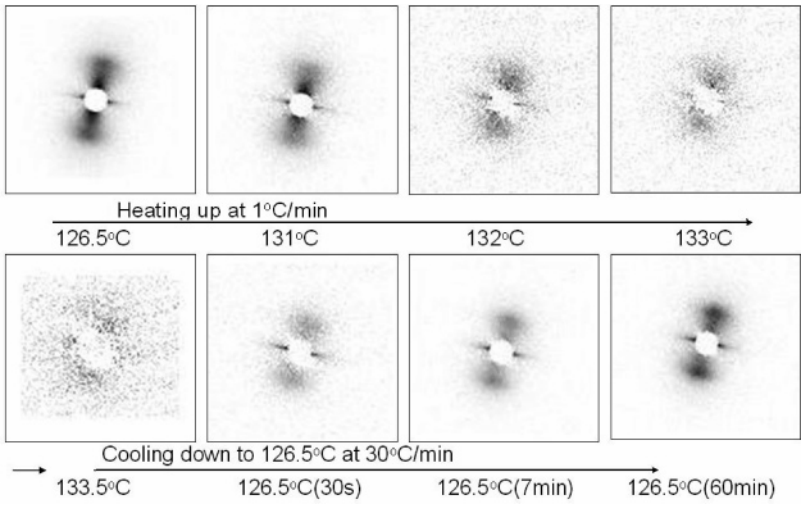

Figure 9. Selected 2D SAXS patterns of the LMWPE/HMWPE blend during the first thermal cycle (the patterns shown above were taken after 5 min hold at the corresponding temperature).

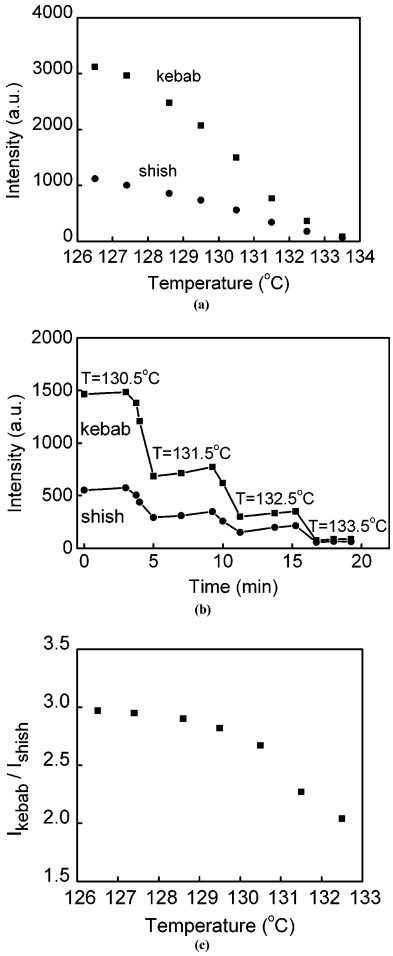

Figure 10. (a) Integrated SAXS intensities from shish and kebabs at the end of each holding temperature in the first thermal cycle. (b) Time evolution of integrated SAXS intensities from shish and kebabs at the late stage of the first thermal cycle. (c) The ratio of I_{kebab} to I_{shish} at the end of each holding temperature in the first thermal cycle.

Since crystallization was carried out at the same temperature (126.5 °C) and the same duration (1 h) for both stages, the lamellar thickness (which is a strong function of supercooling) should remain the same. So, the larger long period at the recrystallization indicates that a lesser amount of crystals was formed (i.e., the lamellae were more sparsely spaced). This can be attributed to the reduction in the total amount of the oriented,

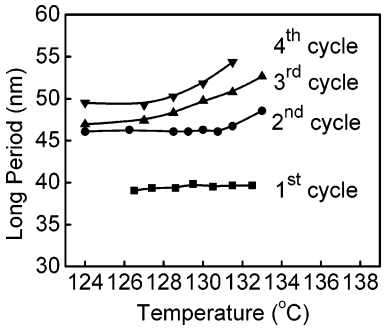

Figure 11. Changes of long periods of shish-kebab structure in the LMWPE/HMWPE blend during the heating stages in the first four thermal cycles.

crystallizable chain segments after the melting process. However, we envision that some chains indeed completely relax and cannot participate in the recrystallization process.

The second thermal cycle was carried out at the end of 60 min recrystallization at 126.5 °C (immediately after the end of the first cycle). As mentioned in the Experimental Section, in second and subsequent cycles, the sample was not subjected to stepwise heating; instead, it was heated continuously to the highest temperature of the corresponding cycle at a 3 °C/min rate (see Figure 2; for example, 136 °C in the second cycle). During heating in the second cycle, the observed melting behavior was very similar to that in the first cycle. Both scattered intensities from shish and kebabs decreased with the increase of temperature. It was found that the long period remained about constant (46 nm) before 131 °C, and it started to increase afterward (Figure 11), again due to the relaxation/nonparticipation of some of the chains in the recrystallization process. The final long period was 48.5 nm at 133 °C; beyond 133 °C, it was difficult to determine the long spacing due to the weak meridional maximum.

The subsequent cycles showed similar trends in the shish and kebab intensities as well as the long period. In the third and fourth thermal cycles, the initial scattered intensities of shish and kebabs all became lower, due to the reduction in the total mass fraction of the shish-kebab structure after each thermal cycle. In the third cycle, the scattered intensity of the kebabs decreased rapidly during heating, and it approached zero at 132 °C, whereas the corresponding long period, illustrated in Figure 11, increased immediately upon heating. Generally speaking, the long period increased with the order of the thermal cycles

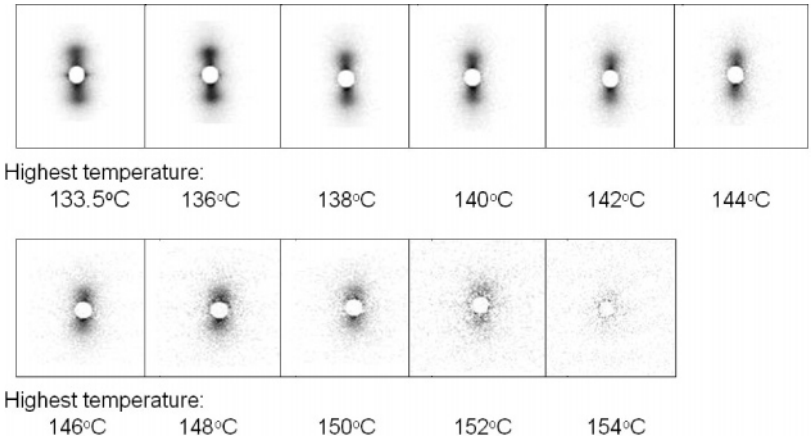

Figure 12. Selected 2D SAXS patterns collected at the end of recrystallization in each thermal cycle. The temperature shown below the pattern is the highest temperature during the heating stage in corresponding thermal cycle. The crystallization temperature is 126.5 °C for the first cycle and 124 °C for others.

at the same final crystallization temperature. The long period changes during cooling in the third and fourth cycles were similar to that in the second cycle, except for a larger initial long period at the beginning of cooling in the high-order cycle.

Figure 12 illustrates the final SAXS patterns collected at the end of recrystallization in all thermal cycles (note that the crystallization temperature was 126.5 °C for the first cycle and 124 °C for all other cycles). In this figure, the equatorial streak could still be seen in the first two patterns (i.e., the first and second cycles with the highest temperature of 133.5 and 136 °C, respectively), but the later patterns only exhibited a meridional scattering feature. The scattered intensity decreased notably after each cycle. In the later cycles, since crystallization took place at the same temperature (124 °C) for the same duration of time (10 min), the decrease in scattered intensity could be attributed to the decreasing number of primary nuclei (from the stretched chain segments) for creation of kebabs. The final SAXS pattern at the end of 11th thermal cycle did not show any sign of the shish-kebab structure. This cycle had the highest temperature of 154 °C; thus, it appears that here the complete relaxation of the stretched chain segments (or the deformed entanglement network) took place. The long period and integrated scattered intensities (total, shish, and kebabs) determined from the final SAXS pattern obtained after each cycle are plotted as a function of the highest temperature in the cycle in parts a and b of Figure 13, respectively. It was found that the long period increased in the first six cycles. (No long period could be identified after heating about 144 °C as there was no indication of scattering maximum, but some meridional scattering feature persisted.) The decrease in the scattered intensity in Figure 13b confirmed that the fraction oriented shish-kebab structure decreased after each thermal cycle.

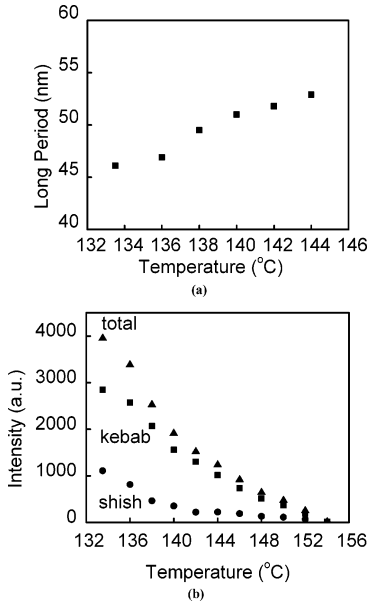

Figure 13. Long periods (a) and integrated SAXS intensities from shish, kebabs, and total (b) obtained after recrystallization as a function of the highest equilibrium temperatures. The crystallization temperature is 126.5 °C for the first cycle and 124 °C for others.

Discussion

The Shish-Kebab Formation from HMWPE Chains. One of the unique features in this study is the careful selection of molecular weight, polydispersity and molecular architecture for the two polyethylene samples. As shown in Figure 1, $\bar{M}_w$ of LMWPE was about 53 000 g/mol, having a polydispersity of 2.2, and $\bar{M}_w$ of HMWPE was 1 500 000 g/mol, having a polydispersity of 1.1. Both samples do not overlap in the molecular weight region at around 300 000 g/mol, which is near the critical orientation molecular weight at the similar degree of supercooling, as estimated from our previous work for PE and iPP.[30,31,35] As LMWPE is a random copolymer of ethylene (98 mol %) and hexane (2 mol %), it does not crystallize at the experimental temperatures (i.e., ≥124 °C). In addition, at the chosen shear conditions (temperature = 126.5 °C, shear rate $\dot{\gamma}$ = 125 s^{-1}), the characteristic relaxation times, i.e., the Rouse time, τ_R, chain disentanglement or reptation time, τ_d, of the LMWPE chains are significantly shorter than the experimental time scale (i.e., $1/\dot{\gamma}$),[38,39] indicating that all relatively short matrix chains would relax back to the coiled state after shear. Thus, the LMWPE matrix behaves mainly as a polymeric solvent, where the only crystallizing component is HMWPE. This hypothesis is further supported by both SAXS and WAXD results.

The development of crystalline shish and kebab structures, all from the narrow distribution of HMWPE chains, requires explanation of rational molecular mechanism. In the supercooled melt, HMWPE chains are in the entangled state, whose entanglement density is mainly a function of concentration but not of temperature.[40] In other words, the average segment length between the entanglement points (or the entanglement molecular weight M_e) does not change with temperature but change with concentration. Thus, the entanglement density of the chosen blend (2 wt % HMWPE) should remain about constant under all experimental conditions (i.e., during and after shear). There

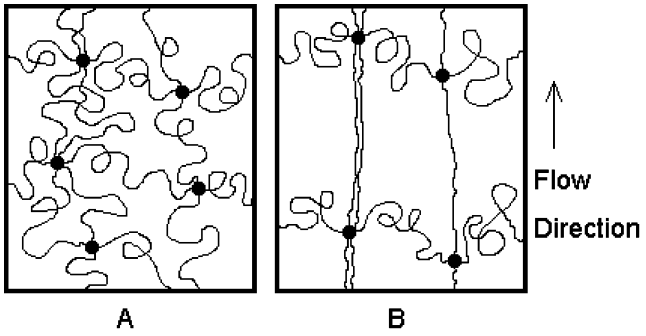

Figure 14. Schematic representation of the entanglement network of HMWPE chains (A) under uniaxial deformation (LMWPE chains are not shown here). Upon shearing, some chain segments between entanglements (shown as round dots) are stretched along the flow direction, but most segments remained in the coiled state (B). The stretched segments form the precursors for the shish formation, and the coiled segments can grow into kebabs.

are several characteristic time scales that determine the state of orientation and extension for chain segments between the entanglement points in HMWPE during and after cessation of shear. These time scales include (1) the imposed shear (flow) time scale (τ_{exp}), which is inversely proportional to the shear rate ($\tau_{exp} \propto \dot{\gamma}^{-1}$), (2) the Rouse time ($\tau_R$), which is related to the relaxation of the chain segments between the entanglement points, and (3) the reptation time (τ_d), which is related to the relaxation of monodispersed chain.[38,39] In addition, there are other "breathing" modes, such as contour length fluctuation (CLF) and convective constraint release (CCR), that can relax chain or segment orientation. At very low shear rates or $\tau_{exp} \gg \tau_d$, reptation along with CLF dominates the relaxation process, and almost no chain segments should remain oriented; here the stretched state is, obviously, not at all possible. At intermediate shear rates or $\tau_{exp} \sim \tau_d$, the chain segments between the entanglements can be oriented but not stretched. At very high shear rates or when $\tau_R > \tau_{exp}$, the chain segments between the entanglements can be both oriented and stretched. At the chosen shear conditions, the scenario of $\tau_R > \tau_{exp}$ (= 0.08 s) must have been met: the evolution of shish evidence straight or oriented and stretched chain sections between the entanglement points. This scenario will be further discussed elsewhere. It is clear that the crystallization process will also alter the state of the entanglement topology. That is, in the crystalline region, the entanglement is largely eliminated; however, the entanglement density should increase in the amorphous region surrounding the lamellae.

If one considers the entangled melt as a network structure, containing entanglement points at dynamic equilibrium as physical cross-links, then the deformation field (i.e., flow) would generate two populations of chain segments conformation, as illustrated in Figure 14: (1) stretched segments oriented along the flow direction and confined by the entanglement points and (2) unoriented and unstretched segments (or coiled segments) perpendicular to the flow direction. Unlike the deformation of chemically cross-linked network material, the extent of the stretched segments in the entangled melt under flow is also a function of strain rate. Under the supercooled state, both stretched and coiled segments can crystallize, most likely following the pathway proposed by Muthukumar et al. for monodispersed stretched and coiled chains.[18] That is the stretched segments can rapidly crystallize into shish with extended-chain conformation (we note that the characteristic time scale of extended-chain crystallization should be order of magnitudes faster than the experimental time scale or the relaxation time scale in entangled HMWPE chains), and the coiled segments can crystallize into the kebabs with folded-chain conformation. Muthukumar et al. have predicted that the growth rate (G) of kebabs should follow a diffusion-controlled mechanism (i.e., $G \propto t^{-0.5}$). This prediction is consistent with our experimental observations that the (overall) kebab growth rate from coiled HMWPE chain segments was indeed not constant. The difference between the predicted exponent of -0.5 (i.e., for diffusion-controlled growth under ideal conditions) and the experimental exponent of -0.76 may be due to the connectivity of chain segments in the entangled melt or the possible difference between the growths of microkebabs and macrokebabs. The latter hypothesis is not clear and will be the subject of our future study.

Thermal Stability of the Shish-Kebab Structure. During heating in the first thermal cycle, we noted the decrease in the

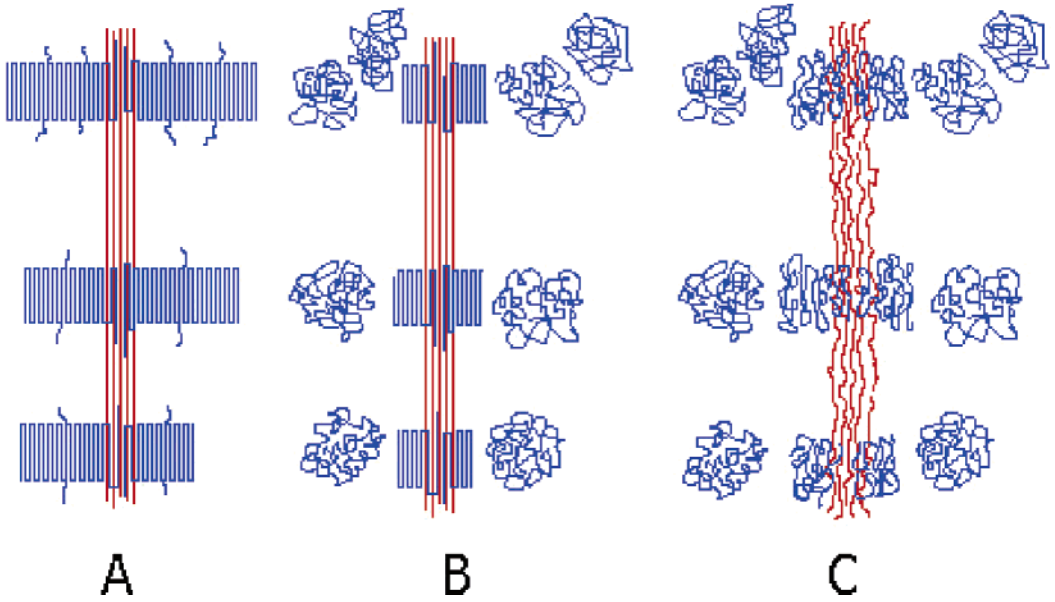

Figure 15. Schematic representation of the shish-kebab structure at the different stages (LMWPE chains are not shown here): (A) stable shish-kebab structure after isothermal crystallization, (B) the melting of macrokebabs during heating, (C) the melting of microkebabs and shish as an integrated entity at a higher temperature. (In (B) and (C), only chain segments are shown and the segment connectivity is omitted.)

I_{shish} and I_{kebab} values as well as in the I_{kebab}/I_{shish} ratio, but a constant long period, with the increase of temperature. On the basis of these observations, we composed a model to describe the thermal stability of the shish-kebab structure (illustrated in Figure 15), modified from the one proposed by Petermann.[27−29] Diagram A represents a well-formed shish-kebab structure before heating. The microkebabs have fractions of chain segments embedding in the shish, while the macrokebabs grow from the microkebab templates perpendicular to the shish. Upon heating, the outer macrokebabs melt first and relax back to the random coil state, but the inner microkebabs persist with the thermally stable shish. Diagram B illustrates the partially melted shish-kebab structure, surrounded by coiled chain segments in the molten state. (Both diagrams B and C omit the chain connectivity between the molten coiled segments and the residual shish-kebab structure.) When the temperature is increased above the nominal melting point, both microkebabs and shish would lose their crystalline registrations. The chain segments melted from microkebabs will relax back into the coiled state, but the chain segmented melted from shish will remain in the stretched state (diagram C), unless the deformed entanglement network structure is relaxed back, due to high temperature or long hold times, to the undeformed initial state. In Figures 14 and 15, we omitted the presence of LMWPE chains because they could not crystallize under the experimental conditions. Since the LMWPE phase was the dominant matrix, the molten amorphous region would consist of both LMWPE (the major component) and HMWPE (the minor component) chains. When the blend was cooled to the experimental temperature (126.5 °C), only HMWPE chains could crystallize, whereas LMWPE chains would remain in the amorphous region, resulting in an increase in the composition ratio for LMWPE.

The relaxation time scale for the stretched chain segments of shish is order of magnitude higher than that of kebabs. The stretched chain segments can quickly recrystallize into crystalline shish, if cooled to low temperatures, which can subsequently nucleate microkebabs. Thus, the residual shish-kebab structure at the end of each cycle is a direct reflection of the state of the stretched and coiled chain segments upon heating under the confined planar constraints to the highest temperature of the cycle. It is seen that the kebab long period increased but the corresponding scattered intensity decreased with the increase of the highest temperature in each cycle (Figures 11 and 12). This can be attributed to the relaxation of the deformed entanglement network, which reduces the extent of the stretched segments after each thermal cycle to a higher temperature. As the amount of the stretched segments decreases, the amount of the shish re-formation would decrease, resulting in a less amount of kebabs and a larger value of long period between kebabs. In the last thermal cycle with the holding temperature of 154 °C for 3 min, the shish and kebabs re-formation did not take place, indicating the complete relaxation of the deformed entanglement network.

We noticed that the final SAXS patterns taken at the end of the first and the second cycles (Figure 12) all exhibited an equatorial streak together with meridional peaks, whereas the rest patterns only showed meridional scattering feature. In our earlier study,[35] we argued that the lack of equatorial streak does not mean that the shish formation did not take place; it simply means that the concentration of the shish might be too low or the diameter of the shish too thin to be detected by SAXS. However, with our recent observation of multiple shish[41] in the shish-kebab structure induced by shear in a similar bimodal blend, we speculate that the appearance of equatorial streak in SAXS may be related to the occurrence of multiple shish, which has a more enhanced contrast than typical single shish. This hypothesis will be thoroughly tested in our future study.

Conclusion

From the shear-induced crystallization study of a special polymer blend containing 98 wt % noncrystallizing LMWPE and 2 wt % narrowly distributed crystallizing HMWPE using in-situ SAXS and WAXD techniques, we obtained several new insights into the formation, melting, and re-formation of the shish-kebab structure under planar constraints. These new insights can be summarized as follows.

1. Under shear flow, stretched and coiled chain segments coexist even in near monodispersed HMWPE chains. The different states of chain segments are caused by the deformation of the network like structure in highly entangled polymer melt with each entanglement point acting as a physical cross-link.

2. The stretched and coiled segments are responsible for the formation of the shish-kebab structure, where the kebab growth seems to follow a diffusion-controlled process, as predicted by Muthukumar et al.[18]

3. Upon heating, the melting of macrokebabs takes place before the melting of microkebabs and shish, which vanish simultaneously as an integrated entity into coiled and stretched chain segments. The shish-kebab structure can re-form upon cooling, mainly due to the survival of stretched chain segments confined by the entanglement points.

4. The re-formed shish-kebab structure directly reflects the state of stretched and coiled segments upon heating under the confined planar constraints. With increase of temperature, the relaxation of the deformed entanglement network results in the decrease in the extent of stretched segments and the shish-kebab fraction and the increase of the kebab long period.

5. Upon thermal annealing at 154 °C for 3 min, no shish-kebab structure could be re-formed, indicating the complete relaxation of the deformed entanglement network.

Acknowledgment. We acknowledge the assistance of Drs. Igors Sics, Carlos A. Avila-Orta, and Lixia Rong for synchrotron SAXS and WAXD experimental setup. We also thank the helpful comments by Drs. J. M. Schultz and M. R. Nobile. The financial support of this work was provided by the National Science Foundation (DMR-0405432).

References and Notes

(1) Keller, A.; Kolnaar, H. W. *Mater. Sci. Technol.* **1997**, *18*, 189.
(2) Ward, I. M. *Structure and Properties of Oriented Polymers*; Wiley: New York, 1975.
(3) Wunderlich, B. *Macromolecular Physics*; Academic Press: New York, 1973; Vol. 2.
(4) Wilkinson, A. N., Ryan, A. J., Eds.; *Polymer Processing and Structure Development*; Kluwer: Dodrecht, 1998.
(5) Eder, G.; Janeschitz-Kriegl, H. *Mater. Sci. Technol.* **1997**, *18*, 268.
(6) Hobbs, J. K.; Humphris, A. D. L.; Miles, M. J. *Macromolecules* **2001**, *34*, 5508.
(7) Bashir, Z.; Odell, J. A.; Keller, A. *J. Mater. Sci.* **1986**, *21*, 3993.
(8) Somani, R. H.; Hsiao, B. S.; Nogales, A.; Srinivas, S.; Tsou, A. H.; Sics, I.; Balta-Calleja, F. J.; Ezquerra, T. A. *Macromolecules* **2000**, *33*, 9385.
(9) Jerschow, P.; Janeschitz-Kriegl, H. *Int. Polym. Process.* **1997**, *12*, 72.
(10) Sherwood, C.; Price, F.; Stein, R. *J. Polym. Sci., Polym. Symp.* **1978**, *63*, 77.
(11) Lagasse, R. R.; Maxwell, B. *Polym. Eng. Sci.* **1976**, *16*, 189.
(12) Vleeshouwers, S.; Meijer, H. *Rheol. Acta* **1996**, *35*, 391.
(13) Duplay, C.; Monasse, B.; Haudin, J. M.; Costa, J. L. *J. Mater. Sci.* **2000**, *35*, 6093.
(14) Seki, M.; Thurman, D. W.; Oberhauser, J. P.; Kornfield, J. A. *Macromolecules* **2002**, *35*, 2583.
(15) de Gennes, P. G. *J. Chem. Phys.* **1974**, *60*, 5030.

(16) Pope, D. P.; Keller, A. *Colloid Polym. Sci.* **1978**, *256*, 751.
(17) Miles, M. J.; Keller, A. *Polymer* **1980**, *21*, 1295.
(18) Dukovski, I.; Muthukumar, M. *J. Chem. Phys.* **2003**, *118*, 6648.
(19) Na, B.; Wang, Y.; Zhang, Q.; Fu, Q. *Polymer* **2004**, *45*, 6245.
(20) Yamazaki, S.; Hikosaka, M.; Toda, A.; Wataoka, I.; Yamada, K.; Tagashira, K. *J. Macromol. Sci., Phys.* **2003**, *B42*, 499.
(21) Isayev, A. I.; Chan, T. W.; Shimojo, K.; Gmerek, M. *J. Appl. Polym. Sci.* **1995**, *55*, 807.
(22) Gutierrez, M. G.; Alfonso, G. C.; Riekel, C.; Azzurri, F. *Macromolecules* **2004**, *37*, 478.
(23) Azzurri, F.; Alfonso, G. C. *Macromolecules* **2005**, *38*, 1723.
(24) Hill, M. J.; Barbam, P. J.; Keller, A *Colloid Polym. Sci.* **1980**, *258*, 1023.
(25) Hill, M. J.; Keller, A. *Colloid Polym. Sci.* **1981**, *259*, 335.
(26) Hill, M. J.; Barbam, P. J.; Keller, A. *Colloid Polym. Sci.* **1983**, *261*, 721.
(27) Liu, T.; Petermann, J.; He, C.; Liu, Z.; Chung, T. *Macromolecules* **2001**, *34*, 4305.
(28) Liu, T.; Lieberwirth, I.; Petermann, J. *Macromol. Chem. Phys.* **2001**, *202*, 2921.
(29) Liu, T.; Tjiu, W. C.; Petermann, J. *J. Cryst. Growth* **2002**, *243*, 218.
(30) Somani, R. H.; Hsiao, B. S.; Nogales, A.; Fruitwala, H.; Srinivas, S.; Tsou, A. H. *Macromolecules* **2001**, *34*, 5902.
(31) Nogales, A.; Hsiao, B. S.; Somani, R. H.; Srinivas, S.; Tsou, A. H.; Balta-Calleja, F. J.; Ezquerra, T. A. *Polymer* **2001**, *42*, 5247.
(32) Keum, J.; Somani, R. H.; Zuo, F.; Burger, C.; Sics, I.; Hsiao, B. S.; Chen, H.; Kolb, R.; Lue, C. *Macromolecules* **2005**, *38*, 5128.
(33) de Gennes, P. G. *Scaling Concepts in Polymer Physics*; Cornell University Press: Ithaca, NY, 1979.
(34) Ballard, D. G. H.; Cheshier, P.; Longman, G. W.; Schelten, J. *Polymer* **1978**, *19*, 379.
(35) Yang, L.; Somani, R. H.; Sics, I.; Hsiao, B. S.; Kolb, R.; Fruitwala, H.; Ong, C. *Macromolecules* **2004**, *37*, 4845.
(36) Somani, R. H.; Hsiao, B. S.; Nogales, A.; Srinivas, S.; Tsou, A. H.; Scis, I.; Balta-Calleja, F. J.; Ezquerra, T. A. *Macromolecules* **2000**, *33*, 9385.
(37) Keum, J.; Burger, C.; Hsiao, B. S.; Somani, R. H.; Yang, L.; Chu, B.; Kolb, R.; Chen, H.; Lue, C. *Prog. Colloid Polym. Sci.* **2005**, *130*, 114.
(38) Milner, S. T.; McLeish, T. C. B. *Phys. Rev. Lett.* **1998**, *31*, 725.
(39) Bent, J.; Hutchings, L. R.; Richards, R. W.; Gough, T.; Spares, R.; Coates, P. D.; Grillo, I.; Harlen, O. G.; Read, J. D.; Garham, R. S.; Likhtman, A. E.; Groves, D. J.; Nicholson, T. M.; McLeish, T. C. B. *Science* **2003**, *301*, 1692.
(40) Doi, M.; Edwards, S. F. *The Theory of Polymer Dynamics*; Oxford Science Publications: Oxford, 1986.
(41) Hsiao, B. S.; Yang, L.; Somani, R. H.; Carlos, A. A.; Zhu, L. *Phys. Rev. Lett.* **2005**, *94*, 117802.

MA052340G